

15. M. K. Wallis, *Astron. Astrophys.* **130**, 200 (1984).
16. V. B. Baranov, M. G. Lebedev, Ju. G. Malama, *Astrophys. J.* **375**, 347 (1991).
17. Ju. G. Malama, *Astrophys. Space Sci.* **176**, 21 (1991).
18. R. Osterbart and H. J. Fahr, *Astron. Astrophys.* **264**, 260 (1992).
19. J. L. Bertaux, J. T. Clarke, M. Mumma, T. Owen, E. Quemerais, in *Science with the Hubble Space Telescope*, European Southern Observatory Conference and Workshop Proceedings No. 44 (1993), p. 459.
20. T. F. Adams and P. C. Frisch, *Astrophys. J.* **212**, 300 (1977).
21. J. T. Clarke, S. Bowyer, H. J. Fahr, G. Lay, *Astron. Astrophys.* **139**, 389 (1984).
22. The GHRS spectrum of sky 2 arc min from Mars was taken with Echelle-A grating and a 2-arc sec aperture in May 1991. The line-of-sight was 42° from the downwind direction for an integration time of 20 min. The red edge of the geocoronal line was estimated by symmetrical reflection of the blue edge. The model line profile has been convolved with a line spread function 0.008 nm wide.
23. Due to the blending with the geocorona at the IUE lower resolution, the red part of the line was preferentially fitted (21). The derived value of 25 km s<sup>-1</sup> is consistent with the broad interplanetary line and the centering at 20 km s<sup>-1</sup> as we observed here.
24. J. L. Bertaux, R. Lallement, V. G. Kurt, E. N. Mironova, *Astron. Astrophys.* **150**, 82 (1985).
25. The hydrogen absorption cell used on the Prognoz spacecraft (24) acts as a kind of negative spectrometer of quasi-infinite resolution, absorbing all the emission within a restricted wavelength range smaller than the Ly- $\alpha$  linewidth. The Doppler shift between the earth and the inflowing gas changes when viewing in different directions provides a modulation of the absorption fraction. From the observed modulation and through modeling of the flow, the initial velocity is 20 km s<sup>-1</sup>.
26. The first number refers to the simple Parker type (18), assuming the LIC flow is submagnetosonic, and the second to the so-called two-shocks model (16, 17), which is relevant for a supermagnetosonic flow. In the former case, a deceleration of 2 km s<sup>-1</sup> is obtained with a plasma density of 0.02 cm<sup>-3</sup> (18). In the latter case, a deceleration of 14 km s<sup>-1</sup> is obtained with a plasma density of 0.2 cm<sup>-3</sup> [R. Lallement *et al.*, *Astrophys. J.* **396**, 696 (1992)]. In the two models the neutral hydrogen density is of the same order (0.1 and 0.07 cm<sup>-3</sup>, respectively).
27. W. S. Kurth, D. A. Gurnett, F. L. Scarf, R. L. Poynter, *Nature* **312**, 27 (1984).
28. A. Czechowski and S. Grzedzielski, *ibid.* **344**, 640 (1990).
29. J. R. Jokipii, in *Physics of the Outer Heliosphere*, S. Grzedzielski and D. E. Page, Eds. (Pergamon, Oxford, 1990), pp. 169–178.
30. R. B. McKibben, in *ibid.*, pp. 107–118.

19 January 1993; accepted 30 March 1993

## Slow Magnetic Relaxation in Iron: A Ferromagnetic Liquid

R. V. Chamberlin and M. R. Scheinfein

The remanent magnetization of single-crystal iron whiskers has been measured from 10<sup>-5</sup> to 10<sup>4</sup> seconds after the removal of an applied field. The observed response is accurately modeled by localized magnon relaxation on a Gaussian size distribution of dynamically correlated domains, virtually identical to the distribution of excitations in glass-forming liquids. When fields of less than 1 oersted are removed, some relaxation occurs before 10<sup>-5</sup> second has elapsed; but when larger fields are removed, essentially all of the response can be accounted for by magnon relaxation over the available time window. The model provides a physical picture for the mechanism and observed distribution of Landau-Lifshitz damping parameters.

The Landau-Lifshitz-Gilbert equations govern all classical ferromagnetic response mechanisms (1–3). Relaxation toward the local internal magnetic field ( $H_1$ ) is characterized by a dimensionless Landau-Lifshitz damping parameter  $\alpha$ , which connects the free-electron gyromagnetic ratio,  $\gamma = 1.76 \times 10^7 \text{ s}^{-1} \text{ Oe}^{-1}$ , to the observed relaxation rate,  $1/\tau = \alpha\gamma H_1$  (note, 1 Oe =  $10^3/4\pi \text{ A m}^{-1}$ ; or, in vacuum,  $H = 1 \text{ Oe}$  produces  $B = 1 \text{ G}$ ). Experimental values of  $\alpha$  (~0.01) are usually determined from ferromagnetic resonance linewidths in  $H_1 \sim 1 \text{ kOe}$  (4, 5), so that gyromagnetic precession occurs at microwave frequencies and  $\tau \sim 10^{-9} \text{ s}$ . Here we report magnetic relaxation measurements of single-crystal Fe whiskers in very low residual fields ( $H_1 < 1 \text{ mOe}$ ), so

that  $\tau \sim 10^{-3} \text{ s}$  is within the time window of our superconducting quantum interference device (SQUID) magnetometer. The primary response is accurately modeled by a Gaussian size distribution of localized internal degrees of freedom (localized magnons), virtually identical to the distribution of excitations in glass-forming liquids (6, 7). The model provides a physical picture for the mechanism and observed distribution of Landau-Lifshitz damping parameters.

Classical ferromagnetic response mechanisms include domain switching, wall motion, and magnon relaxation (8, 9). Domain walls usually move quite rapidly, so that an equilibrium configuration is achieved within 10<sup>-6</sup> s. Most previous models for the “slow” ( $t > 10^{-5} \text{ s}$ ) response in magnetic rocks (10), spin glasses (11, 12), and ferromagnets (13, 14) have considered domain switching (domain inver-

sion by means of activation over an intermediate barrier), where large domains with large barriers relax slowly. The key distinction of our approach is that we consider the response of low-energy, internal degrees of freedom (examples include magnons, phonons, and polaritons) for which the energy-level spacing decreases with increasing domain size. Our model gives better agreement with the observed response from dozens of different materials, including magnetic relaxation in random ferromagnets, spin glasses, and oxide superconductors (7, 15) as well as the dielectric response or structural relaxation of liquids, glasses, polymers, and metals (6, 7, 16). Here we show that this model accurately describes the primary magnetic response of single-crystal Fe.

Although magnon-like internal degrees of freedom have been shown to dominate the slow relaxation of ferromagnetic EuS (17), the observed response was less than 2% of the initial (in-field) magnetization; most of the relaxation occurred within 10<sup>-5</sup> s. Furthermore, negligible domain switching might have been anticipated because EuS has highly isotropic localized spins with poorly defined static domain structure. In contrast, single-crystal Fe whiskers have well-defined macroscopic domains; hence, switching and wall motion should appear as conspicuous jumps in the net magnetization during relaxation.

We have measured the magnetization of single-crystal Fe whiskers from 10<sup>-5</sup> to 10<sup>4</sup> s after removing an applied field,  $H$ . For  $H < 3 \text{ Oe}$ , only smooth relaxation is observed. Small jumps ( $< \pm 2\%$ ) appear when  $H > 3 \text{ Oe}$ , but they do not contribute significantly to the otherwise smooth response; essentially, all of the net change in magnetization can be accounted for by localized magnon relaxation over the range 10<sup>-5</sup> to 10<sup>-2</sup> s, consistent with the observed distribution and expectedly slow Landau-Lifshitz damping rates.

Single-crystal Fe whiskers are often investigated as an ultrapure form of Fe (18). High-quality whiskers have a square cross section with length [(100)-direction] much longer than width. Typical dimensions are 5 mm by 0.1 mm by 0.1 mm. The static magnetic domain configuration consists of aligned regions that orient in diverse directions to minimize the net dipolar energy of the sample. In zero field, a typical Fe whisker may contain four macroscopic domains: one oriented longitudinally up one side of the whisker, another oriented down the other side, and one small closure domain at each end (19, 20). In a small magnetic field applied along the axis of the whisker, the domain that is oriented in the direction of  $H$  grows at the expense of the oppositely oriented domain (21, 22). In

Department of Physics and Astronomy, Arizona State University, Tempe, AZ 85287–1504.

higher fields, the opposing domain breaks up into smaller, orthogonally oriented domains. Eventually, above saturation ( $H_s \approx 3$  Oe), the sample forms a single domain oriented in the direction of  $H$ .

Dynamic measurements are sensitive to dynamic correlations, which are generally independent of static alignment. Persistent dynamic correlations exist, even in spin glasses above their freezing temperature (23) and in ferromagnets at up to three times their Curie temperature (24, 25). The model that accurately characterizes the observed relaxation of Fe requires a broad distribution of dynamic correlations, which suggests that a single ferromagnetically aligned domain contains a myriad of dynamically correlated regions. Experimentally, the distribution of magnons in single-crystal Fe is essentially identical to the distribution of phonons and polaritons in glass-forming liquids (6, 7).

We define a dynamically correlated domain (DCD) as a region in which excitations relax with a single (locally uniform) relaxation rate. Quantum mechanically, a DCD may correspond to a region where particles form a single (coherent) many-bodied system, thus ensuring uniform relaxation throughout the domain. Thermodynamically, a DCD is a canonical system that, during relaxation, need not be in equilibrium with neighboring domains or the thermal bath. Four-dimensional nuclear magnetic resonance (NMR) spectroscopy (26) has demonstrated that the primary response in a glass-forming liquid is caused by a heterogeneous distribution of DCDs. The temperature dependence of the remanent magnetization in EuS (17) confirms that even single-crystal ferromagnets contain interacting, but distinct, dynamically correlated domains.

Dynamic correlations in a ferromagnet may be pictured as follows. At finite temperatures, thermal fluctuations decrease the local magnetization from saturation. A small reduction in energy occurs if two neighboring spins fluctuate coherently, so that they are virtually aligned at all times, not merely when time-averaged. Because this energy reduction is on the order of  $k_B T$ , where  $k_B$  is Boltzmann's constant, these dynamic correlations will be thermally distributed throughout the sample and may influence behavior at all temperatures. For harmonic interactions in a perfect crystal, Bloch's theorem requires that all fluctuations be a linear combination of plane-wave excitations; in real systems, normal-mode excitations (magnons) may be transiently localized into DCDs. In the Landau-Lifshitz formalism, excitations are coherent over the magnetic exchange length (27), which is  $\sim 8$  nm in Fe at low temperatures. Similar dynamical correlations, characteristic of

DCDs, are found in a variety of physical systems (28).

For a DCD-size distribution  $n_s$ , with size-dependent initial response  $M_s$  and relaxation rate  $\omega_s$ , the net relaxation is the weighted sum over all sizes

$$M(t) = \sum_{s=0}^{\infty} M_s n_s e^{-t\omega_s} \quad (1)$$

Here,  $s$  is the number of spins (proportional to volume) in a DCD. Some physically reasonable assumptions are made to obtain the size dependences of  $M_s$ ,  $n_s$ , and  $\omega_s$ .

The equilibrium response per spin ( $M_0$ ) is assumed to be homogeneous,  $M_s = M_0 s$ . The relaxation rate of each DCD is assumed to obey activated (Arrhenius-like) behavior,  $\omega_s \propto e^{-\delta E_s/k_B T}$ . The key assumption is that we consider low-energy, internal degrees of freedom for which the density of states is proportional to volume  $\delta N/|\delta E_s| \propto s$ , so the energy difference between adjacent ( $\delta N = 1$ ) energy levels is  $\delta E_s = \pm \Delta/s$  (here,  $\Delta$  is an energy bandwidth that is independent of size). Although Fröhlich considered finite size effects in 1937, the thermodynamic requirement that average energy-level spacings must vary as  $\delta E_s \propto 1/s$  was first recognized by Kubo in 1962 (29). We implement this requirement to obtain relaxation rates that vary exponentially with inverse size  $\omega_s = \omega_{\infty} e^{-(\pm \Delta/k_B T)/s}$ , where  $\omega_{\infty}$  is an asymptotic relaxation rate for large domains. Finally, a Gaussian DCD size distribution is assumed, with deviation  $\sigma$  about an average size  $\bar{s}$ ,  $n_s \propto e^{-[(s-\bar{s})/\sigma]^2}$ . With use of  $x = s/\sigma$ , the net relaxation becomes

$$M(t) \propto M_0 \int_0^{\infty} [x e^{-(x-\bar{x})^2}] e^{-t\omega_{\infty} e^{-cx}} dx \quad (2)$$

Four of the parameters are adjustable:  $M_0$  accommodates the magnitude of response,  $\omega_{\infty}$  adjusts the time scale of relaxation, the dynamical correlation coefficient  $C = (\pm \Delta/k_B T)/\sigma$  governs the spectral shape, whereas the (scaled) average domain size  $\bar{x} = \bar{s}/\sigma$  influences the spectrum and time scale of relaxation.

Magnetic relaxation of single-crystal Fe whiskers was measured with a SQUID magnetometer coupled to a high-speed voltmeter. We made measurements by applying a field  $H$  along the (100)-axis of the whisker, waiting several seconds for the sample to attain virtual equilibration, removing  $H$ , and recording the magnetization as a function of time (30). For  $H < 1$  Oe, a small pseudologarithmic relaxation was visible at long times. The behavior of this relaxation (which accounts for less than 5% of the total response from  $10^{-5}$  to  $10^4$  s) is identical to the relaxation observed in EuS at low temperatures (17). This small "logarithmic background" and a constant base-

line have been subtracted from all relaxation data presented here.

The size-dependent weight factor  $x^{1-\theta} e^{-(x-\bar{x})^2}$  used in Eq. 2 assumes homogeneous response ( $1 - \theta = 1$ ) and a random distribution of domain volumes ( $\zeta = 1$ ). If response was attributable to domain walls or if domain radius was the relevant randomness parameter, then one would expect  $1 - \theta = 2/3$  or  $\zeta = 1/3$ , respectively. When data of sufficient quality and range are fit,  $1 - \theta$  and  $\zeta$  may be released as additional adjustable parameters, so that size scaling is solely established by the inverse-linear behavior in the exponent of the relaxation rate,  $\omega_x = \omega_{\infty} e^{-C/x}$ . From the magnetic relaxation of Fe,  $1 - \theta = 0.92 \pm 0.12$  and  $\zeta = 0.99 \pm 0.08$ . Excellent agreement with the exact predictions quantitatively confirms all assumptions of the model: homogeneous response, Gaussian distribution of excitation volumes, and relaxation rates that vary exponentially with inverse size (otherwise,  $1 - \theta$  and  $\zeta$  would deviate to compensate). Empirically, within experimental resolution, Eq. 2 is the correct response function for these data.

In principle, both  $\bar{x}$  and  $C$  can accommodate variations in the spectral shape of Eq. 2; but experimentally their ratio from magnetic relaxation in Fe,  $\bar{x}/C = 0.197 \pm 0.02$ , is indistinguishable from  $\bar{x}/|C| = 0.19 \pm 0.02$ , the value found for the stress relaxation and dielectric susceptibility of a wide variety of glass-forming liquids (7). This Gaussian distribution of DCD sizes has been shown (6) to indicate long-ranged randomness, characteristic of ergodic systems ("liquids"). Experimentally, with the use of  $\bar{x} = 0.19|C|$ , Eq. 2 accurately characterizes the observed relaxation in Fe and other "liquids" with a single adjustable parameter governing the entire spectrum of response.

The remanent magnetization as a function of time after the removal of the various applied fields (at 4.2 K) is shown in Fig. 1. Considerable relaxation occurs between  $10^{-5}$  and  $10^{-2}$  s. Measurements at higher temperatures (up to 40 K) show virtually the same behavior with no significant change in the magnitude or rate of relaxation. Presumably, such clear primary response in Fe whiskers has not previously been reported (31) because most SQUID magnetometers are incapable of making measurements on these time scales. For  $H < 3$  Oe (Fig. 1A), Eq. 2 with  $\bar{x} = 0.19C$  gives excellent agreement with the observed relaxation. The primary deviation of the data from Eq. 2 is attributable to digitizing noise (Fig. 1A, inset). For  $H > 3$  Oe (Fig. 1B), small Barkhausen jumps (domain-wall adjustments between local pinning sites) appear in the available time window, but they do not contribute signif-

icantly to the net response. For all initially applied fields, Eq. 2 is the correct function for the primary observed response; in Fe, magnetic relaxation is governed by localized magnons on a Gaussian size distribution of independently relaxing domains.

Magnetic susceptibility as a function of frequency (Fig. 2, A and B) is given by the Fourier transform of  $-d(M/H)/dt$ . Using Eq. 2, we find

$$\chi(\omega) \propto M_0 \int_0^{\infty} [x e^{-(x-\bar{x})^2}] \frac{1 + i\omega/w_x}{1 + (\omega/w_x)^2} dx \quad (3)$$

Observed peak absorption frequencies ( $\nu_p = \alpha\gamma H_1/2\pi$ ) are consistent with a net internal field of  $H_1 \sim H_0$  and the known gyromagnetic ratio  $\gamma = 1.76 \times 10^7 \text{ s}^{-1} \text{ Oe}^{-1}$  and average Landau-Lifshitz damping parameter ( $\alpha \approx 0.01$ ) of Fe. The model provides a physical picture for the mechanism and observed distribution of  $\alpha$ . The deviations of the 65-Oe data from Eq. 2 (Fig. 2C) generally occur more slowly than  $\nu_p$ , consistent with minor readjustments of domain walls in response to the dominant magnon relaxation.

Some relaxation occurs before the available time window. The total response attributable to magnon relaxation may be determined by extrapolation of fits from Eq.

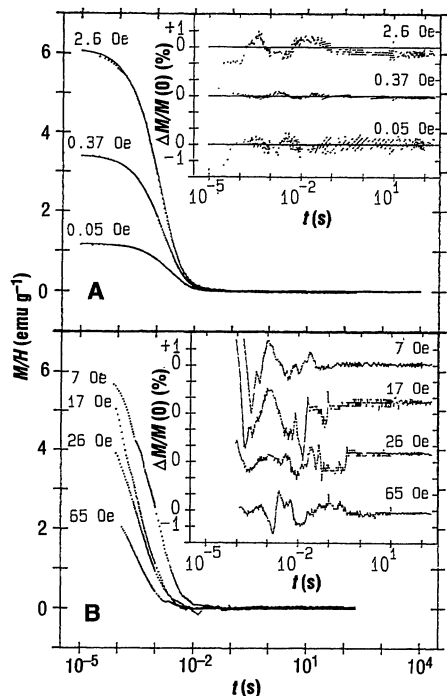


**Fig. 1.** Magnetization of an Fe whisker, measured in electromagnetic units (emu) per gram, at 4.2 K as a function of time after removal of a field  $H$ . Curves are labeled with values of  $H$  and are split into (A)  $H < 3$  Oe and (B)  $H > 3$  Oe. (Inset) Difference between the data and a model for independently relaxing, localized excitations (Eq. 2 with  $\bar{x} = 0.19C$  where  $C = 30 \pm 5$ ).

2 to  $t = 0$ . At  $H = 0.05$  Oe, the response directly attributable to magnons is about 20% of the in-field magnetization (Fig. 3A); 80% of the relaxation occurs before  $10^{-5}$  s has elapsed, which is possibly attributable to domain switching, wall motion, or isolated spin excitations. The fraction of response accurately accounted for by Eq. 2 increases with increasing field until  $H > 1$  Oe, where essentially 100% of the relaxation is attributable to magnon response. Apparently, because the relaxation rate  $\alpha\gamma H_1$  is so slow, domain walls (which traverse the sample within the first  $10^{-5}$  s) cannot carry any magnetization reversal. Instead, these "proto-walls" merely break the symmetry between regions of the sample where magnons will eventually relax the magnetization toward distinct directions; zero-field alignments evolve smoothly from high-field saturation without significant contribution from wall motion.

The asymptotic relaxation rate increases with increasing magnetic field (Fig. 3B). An intrinsic relaxation rate should not vary significantly with  $H$  (because relaxation occurs in  $H_1 \approx H_0$ ), which suggests that the observed  $H$  dependence must be the result of changes in average DCD size through  $(\Delta/k_B T) = \bar{s}/0.19$  in  $w_\infty = w_0 e^{(\Delta/k_B T)/s_0}$ . Here,  $w_0$  is an intrinsic relaxation rate, corresponding to a DCD of size  $s_0$ . Presumably,  $s_0$  is the minimum size for which dynamic correlations can relax coherently ( $s_0 \geq 1$ ), but it is sufficient to assume that  $s_0$  is some fixed size. The average DCD size

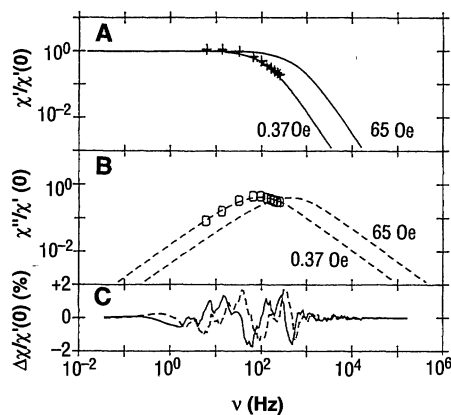


**Fig. 2.** Normalized (A) real and (B) imaginary components of the magnetic susceptibility of Fe as a function of frequency as determined from data in Fig. 1. The symbols are from the direct measurements of Heinrich and Arrott (35) [after reduction of the frequency scale by a factor of 750, which may (36) be attributable to the fact that they were made in the earth's field  $H_0 \approx 0.5$  Oe, whereas the residual field of our magnetometer is  $H_0 \approx 0.8$  mOe]. (C) Frequency spectrum of deviations of the real (solid line) and imaginary (dashed line) components of the 65-Oe data from Eq. 2 [numerical Fourier transform of  $-d[\Delta M/M(0)]/dt$  from inset of Fig. 1B].

should increase with increasing  $H$  because magnetic fields reduce fluctuations.

Changes in  $\bar{s}$  may be deduced from Eq. 2 as follows: Because  $\bar{x}^2 \approx 30 \gg 1$ , the lower limit on the integral may be extended to  $-\infty$ , yielding  $M(t=0) \propto M_0 \bar{s}$ . Thus, the average DCD size is proportional to the observed initial response, normalized by the expected intrinsic response  $\bar{s} \propto M(0)/M_0$ . The value of  $M(0)$  is determined experimentally from fits to relaxation data (Fig. 3A). Below saturation ( $H < 10$  Oe), demagnetization limits the intrinsic response to  $M_0 \propto H$  (32); whereas for  $H > 10$  Oe the expected response of a single, statically aligned domain is  $M_0 \propto \sqrt{H}$  (33, 34). The ratio  $M(0)/M_0$  increases logarithmically with field, consistent with  $\bar{s} \propto 4.5 + 2.6 \log(H)$  (Fig. 3C). This DCD growth suggests that  $w_\infty$  should have a power law field dependence:  $w_\infty = 8.2 \times 10^4 H^{0.27} \text{ s}^{-1}$  (Fig. 3B). Deviations of  $w_\infty$  from the power law predicted by DCD growth could be a result of nonlinear demagnetization effects in the vicinity of the saturation field. Thus, measured time and field dependences of the

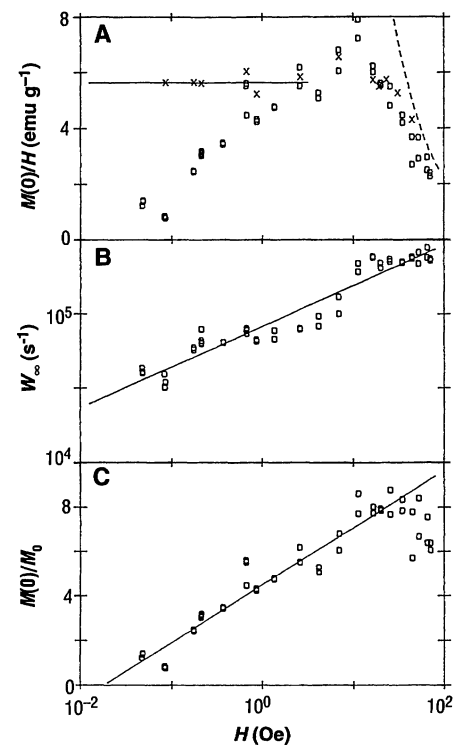


**Fig. 3.** Field dependence: (A) In-field susceptibility  $M/H$  ( $\times$ ) (from before  $H$  was removed) and extrapolated initial response  $M(0)/H$  ( $\square$ ). The low-field susceptibility (32) is  $M/H = 5.6 \text{ emu g}^{-1}$  (solid line); the saturation magnetization is  $M_s = 223 \text{ emu g}^{-1}$  (dashed curve). (B) Asymptotic relaxation rate  $w_\infty$ . Fit to a power law (solid line) yields  $w_\infty = 8.2 \times 10^4 H^{0.27} \text{ s}^{-1}$ . (C) Average domain size,  $\bar{s} \propto M(0)/M_0$ . The assumed intrinsic response is  $M_0 \propto H$  for  $H < 10$  Oe and  $M_0 \propto \sqrt{H}$  for  $H > 10$  Oe. The best linear fit (solid line) yields  $\bar{s} \propto 4.5 + 2.6 \log(H)$ .

primary magnetic response of single-crystal Fe whiskers are accurately characterized by a model for localized magnons on a Gaussian size distribution of independently relaxing domains.

## REFERENCES AND NOTES

1. T. H. O'Dell, *Ferromagnetodynamics* (Wiley, New York, 1981).
2. R. H. Victora, *Phys. Rev. Lett.* **58**, 1788 (1987).
3. D. D. Awschalom, D. P. DiVincenzo, J. F. Smyth, *Science* **258**, 414 (1992).
4. A. D. Berk, *J. Appl. Phys.* **28**, 190 (1957).
5. D. S. Rodbell, *ibid.* **30**, 187S (1959).
6. R. V. Chamberlin, R. Böhmer, E. Sanchez, C. A. Angell, *Phys. Rev. B* **46**, 5787 (1992).
7. R. V. Chamberlin and M. R. Scheinfein, *Ultramicroscopy* **47**, 408 (1992).
8. C. Kittel and J. K. Galt, *Solid State Phys.* **3**, 437 (1956).
9. B. D. Cullity, *Introduction to Magnetic Materials* (Addison-Wesley, Menlo Park, CA, 1972), chap. 12.
10. L. Néel, *Ann. Geophys.* **5**, 99 (1949); *Adv. Phys.* **4**, 191 (1955).
11. A. P. Malozemoff and E. Pytte, *Phys. Rev. B* **34**, 6579 (1986).
12. D. S. Fisher and D. A. Huse, *Phys. Rev. Lett.* **56**, 1601 (1986).
13. E. C. Stoner and E. P. Wohlfarth, *Philos. Trans. R. Soc. London* **240**, 599 (1948).
14. R. H. Victora, *Phys. Rev. Lett.* **63**, 457 (1989).
15. R. V. Chamberlin and D. N. Haines, *ibid.* **65**, 2197 (1990).
16. ———, D. W. Kingsbury, *J. Non-Cryst. Solids* **131–133**, 192 (1991).
17. R. V. Chamberlin and F. Holtzberg, *Phys. Rev. Lett.* **67**, 1606 (1991).
18. S. S. Brenner, *Acta Metall.* **4**, 62 (1956).
19. C. Kittel, *Phys. Rev.* **70**, 965 (1946).
20. R. W. de Blois and C. D. Graham, Jr., *J. Appl. Phys.* **29**, 931 (1958).
21. H. J. Williams, W. Shockley, C. Kittel, *Phys. Rev.* **80**, 1090 (1950).
22. R. V. Coleman and G. F. Scott, *ibid.* **107**, 1276 (1957).
23. F. Mezei, *J. Magn. Magn. Mater.* **31–34**, 1327 (1983).
24. ———, *Phys. Rev. Lett.* **49**, 1096 (1982).
25. H. G. Bohn, A. Kollmar, W. Zinn, *Phys. Rev. B* **30**, 6504 (1984).
26. K. Schmidt-Rohr and H. W. Spiess, *Phys. Rev. Lett.* **66**, 3020 (1991).
27. M. E. Schabes and H. N. Bertram, *J. Appl. Phys.* **64**, 1347 (1988).
28. P. Choquard and J. Clerouin, *Phys. Rev. Lett.* **50**, 2086 (1983).
29. R. Kupo, *J. Phys. Soc. Jpn.* **17**, 975 (1962).
30. The  $H$  solenoid had a time constant of  $\sim 3 \times 10^{-6}$  s, after which  $\mu$ -metal and superconducting shields reduced the residual field to  $H_0 \approx 0.8$  mOe. Net magnetization in the (100)-direction was measured by concentric, second-order gradiometer, flux-transformer coils connected to the SQUID. Absolute magnetization was determined before and after each relaxation by movement of the sample between two of the counterwound coils.
31. C. Heiden and H. Rogalla, *J. Magn. Magn. Mater.* **19**, 240 (1980).
32. In Fig. 3A, for  $H > 10$  Oe,  $M/H$  approaches saturation,  $M_s = 223$  emu  $g^{-1}$ . For  $H < 10$  Oe, the demagnetization factor ( $N/4\pi = 0.00144$  for an aspect ratio of 50:1) limits the net magnetization to  $M/H = 1/N \approx 55$  emu  $cm^{-3} \approx 5.6$  emu  $g^{-1}$ . Thus, below saturation, demagnetization reduces the net internal field by a factor  $H_i/H \approx 0.3$ , which is estimated from the ratio of measured to known magnetization at saturation  $M(H_s)/M_s \approx (6.5 \times 10)/223 \approx 0.3$ , consistent with the ratio of known to apparent saturation fields  $H_s/10 \approx 0.3$ .
33. T. Holstein and H. Primakoff, *Phys. Rev.* **58**, 1098 (1940).
34. R. Pauthenet, *J. Appl. Phys.* **53**, 2029 (1982).
35. B. Heinrich and A. S. Arrott, *Can. J. Phys.* **50**, 710 (1972).
36. Eddy currents could influence the net relaxation rate, but our observation of no change between 4 and 40 K indicates that the temperature-dependent resistivity [G. R. Taylor, A. Isin, R. V. Coleman, *Phys. Rev.* **165**, 621 (1969)] does not play a role.
37. We thank A. S. Arrott for supplying the Fe whiskers, which were grown at Simon Fraser University (Burnaby, British Columbia) under an operating grant from the Natural Sciences and Engineering Research Council of Canada. We have benefited from conversations with M. A. Glaser, O. F. Sankey, K. E. Schmidt, and R. H. Victora. This research was supported by Office of Naval Research contract N00014-88-K-0094.

kers, which were grown at Simon Fraser University (Burnaby, British Columbia) under an operating grant from the Natural Sciences and Engineering Research Council of Canada. We have benefited from conversations with M. A. Glaser, O. F. Sankey, K. E. Schmidt, and R. H. Victora. This research was supported by Office of Naval Research contract N00014-88-K-0094.

1 December 1992; accepted 9 March 1993

## South Asian Summer Monsoon Variability in a Model with Doubled Atmospheric Carbon Dioxide Concentration

Gerald A. Meehl\* and Warren M. Washington

Doubled atmospheric carbon dioxide concentration in a global coupled ocean-atmosphere climate model produced increased surface temperatures and evaporation and greater mean precipitation in the south Asian summer monsoon region. As a partial consequence, interannual variability of area-averaged monsoon rainfall was enhanced. Consistent with the climate sensitivity results from the model, observations showed a trend of increased interannual variability of Indian monsoon precipitation associated with warmer land and ocean temperatures in the monsoon region.

Variability of the south Asian summer monsoon, of which the Indian monsoon is a major part, is manifested by extreme events (droughts and floods) that have considerable impacts on human society and agriculture. Previous climate-modeling studies have shown greater mean south Asian summer monsoon rainfall attributable to climate change caused by an increase of atmospheric  $CO_2$  concentration (1). However, changes in variability that probably are of greater importance to society (2) have received little attention (3). This is so because global coupled ocean-atmosphere climate models capable of internally generating some aspects of variability of the coupled climate system have only recently been integrated for a sufficient length of time to begin to address such issues. In this report, we describe possible changes to south Asian summer monsoon variability based on a global coupled ocean-atmosphere climate model and compare the results with observations. This comparison allowed us to identify physical processes that may contribute to changes in south Asian monsoon variability in a future  $CO_2$ -enriched climate.

In our simulation, the global atmospheric model had an approximate horizontal resolution of  $4.5^\circ$  latitude by  $7.5^\circ$  longitude and nine vertical levels. Clouds were computed, and soil moisture was parameterized by a simple reservoir formulation. The global ocean model had a coarse grid ( $5^\circ$  by  $5^\circ$ )

and four vertical layers and included a simple thermodynamic formulation for the freezing and melting of sea ice. Coupling between the model components involved sea-surface temperature (SST) from the ocean and net heat flux, freshwater flux, and wind stress from the atmosphere.

The global coupled ocean-atmosphere climate model contains errors that are the products of flaws in each of the components as well as errors compounded by coupled interactions at the air-sea interface (4). The errors in the basic state are representative of the inherent limitations of the current generation of coupled models and reflect our lack of understanding of certain coupled processes in the observed climate system and our inability to fully capture such processes in models. Yet, this model and others like it have been shown to simulate successfully fundamental features of the coupled climate system. Consequently, they have been quite useful for basic  $CO_2$  climate sensitivity studies, for insight into coupled processes in the observed system, and for preliminary indications to policy-makers of possible future climate changes (1, 3). Previous results for  $CO_2$  climate sensitivity (3) and process studies (5) are similar in various models in spite of different formulations, types of model errors, and degrees of model error correction. This similarity suggests that there is a robustness of the climate simulations that gives us a degree of confidence in the results.

Because there are no corrections that force the model climate to the observed

National Center for Atmospheric Research, Boulder, CO 80307–3000.

\*To whom correspondence should be addressed.